Regenerative Therapy 24 (2023) 385–397

Contents lists available at ScienceDirect

Regenerative Therapy

journal homepage: http://www.elsevier.com/locate/reth

Original Article

Comparisons of the effects of silk elastin and collagen sponges on wound healing in murine models

Eiichi Sawaragi [a], Hiroki Yamanaka [a, *], Yuanjiaozi Li [a], Tomo Unzai [b], Shingo Kawabata [c], Takashi Nakano [a], Yasuhiro Katayama [a], Michiharu Sakamoto [a], Yasuhiko Tabata [b], Naoki Morimoto [a]

[a] Department of Plastic and Reconstructive Surgery, Graduate School of Medicine, Kyoto University, Kyoto, Japan
[b] Laboratory of Biomaterials, Institute for Life and Medical Sciences, Kyoto University, Kyoto, Japan
[c] Sanyo Chemical Industries, Ltd., Katsura Research Laboratory, Kyoto, Japan

ARTICLE INFO

Article history:
Received 23 July 2023
Received in revised form
21 August 2023
Accepted 4 September 2023

Keywords:
Angiogenesis
Macrophages
Neoepithelialization
Recombinant proteins
Wound healing

ABSTRACT

Introductions: Silk elastin, a recombinant protein with repeats of elastin and silk fibroin, possesses a self-gelling ability and is a potential wound dressing material. The aim of this study is to elucidate the mechanism of the wound healing-promoting effect of silk elastin by comparing its in vivo behavior in a mouse wound model with that of a collagen sponge.

Methods: Skin defects (8 mm in diameter) were created on the backs of C57BL/6J and BKS.Cg- + Lepr/+Lepr db male mice. Silk elastin sponges of 2.5 or 5.0 mm thickness, as well as collagen sponges, were placed on the wounds and secured with a polyurethane film. In the control group, only the polyurethane film was applied. The remaining wound area was grossly evaluated, and tissue samples were collected after 7, 14, and 21 days for histological evaluation, including neoepithelialization, wound contraction, granulation tissue formation, newly formed capillaries, and macrophages. Genetic analysis was conducted using real-time polymerase chain reaction.

Results: In the study with C57BL/6J, there were no significant differences between the silk elastin and collagen sponge groups. Similarly, in the study using BKS.Cg- + Lepr/+Lepr db, no significant differences were found in the remaining wound area and granulation tissue formation between the silk elastin and collagen sponge groups. However, on day 14, the 5.0-mm-thick silk elastin sponge group showed increased macrophages, longer neoepithelialization, and more frequent angiogenesis compared to other groups. Gene expression of inducible nitric oxide synthase and arginase-1 was also higher in the 5.0 mm thick silk elastin sponge group.

Conclusions: Silk elastin sponges demonstrated superior neoepithelialization and angiogenesis compared to collagen sponges. The results suggest that silk elastin and collagen sponges promote wound healing through different mechanisms, with silk elastin possibly enhancing wound healing by facilitating increased macrophage migration. Further studies are needed, but silk elastin shows great potential as a versatile wound dressing material.

1. Introduction

Effective wound dressings play crucial roles in promoting wound healing. Moist wound healing, as advocated by Winter et al. [1], is now generally accepted and a wide range of wound dressing materials are available [2]. The primary functions of wound dressings are to protect the wound from external stimuli, maintain an adequately moist environment, prevent bacterial growth, and promote healing by stimulating epithelial growth, granulation, and angiogenesis. Currently available types of wound dressing materials include polyurethane films, silicon-based rubber foams, hydrogels, hydrocolloids, alginates, and collagen. Collagen-based wound dressings are often used, especially for full-thickness skin

* Corresponding author.
E-mail address: ymnkahrk@kuhp.kyoto-u.ac.jp (H. Yamanaka).
Peer review under responsibility of the Japanese Society for Regenerative Medicine.

https://doi.org/10.1016/j.reth.2023.09.001

defects, because they provide a scaffolding for cells and promote wound healing by forming capillaries and dermis-like tissue. Examples of collagen-based wound dressings include artificial dermis (e.g., Pelnac® or Integra®). In recent years, collagen/gelatin sponges (CGS) have been reported to be useful in wound healing. When combined with basic fibroblast growth factors, CGS promotes effective wound healing [3,4]. However, collagen-based wound dressings still have certain disadvantages, such as difficulty in application to complex-shaped wounds, weak resistance to bacterial infection, and their animal origin of atelocollagen, which can result in a xeno-immune response in wounds.

To address these issues, we investigated silk elastin (SE) as a novel wound dressing material. SE is an artificial protein with repeats of a silk fibroin sequence—a component of silkworm silk, an elastin sequence, and a bioelastic fiber. It is produced by introducing a plasmid that codes for the SE amino acid sequence into an *E. coli* expression system [5]. In an aqueous solution at a low temperature, the beta-sheet structure is formed via hydrogen bonds between silk fibroin sequences, which are beta-strands [6]. Its structure changes with changes in temperature [7]; in vitro, gelation occurs in approximately 2 h at 37 °C. Subcutaneous and intradermal administration of SE in guinea pigs revealed histological changes, no immune reaction or chronic inflammation, and excellent biocompatibility [8]. It has been developed by Protein Polymer Technologies Ltd. (USA) for applications in tissue engineering and drug delivery. Research and development are underway with this material as it becomes a gel and adheres to the wound surface to maintain a moist environment and promote healing. Kawai et al. reported the effects of SE on wound healing by applying an aqueous SE solution to a mouse model of bedsores and observing its effect on granulation growth and bacterial suppression [9]. Kawabata et al. developed a sponge-shaped SE for clinical use and reported its wound-healing effects [10,11]. Additionally, a physician-led clinical trial of a SE sponge is underway, and its safety has been confirmed in a first in human study [12]. Despite the potential benefits of SE as a wound dressing material, the mechanisms behind its wound-healing properties and its overall mechanism of action remain unclear. In this study, we investigated the mechanisms underlying its wound-healing properties and its overall mechanism of action using a murine wound model and compared with those of a collagen sponge.

2. Materials and methods

2.1. Materials

The following three types of material were used: collagen sponge (Pelnac®, single-layer type, Gunze Co., Ltd., Ayabe, Japan), SE sponge of 2.5-mm thickness, and SE sponge of 5.0-mm thickness (Fig. 1a, b and, c). The two SE sponges were obtained from Sanyo Chemical Industries, Ltd. (Kyoto, Japan). All sponges were prepared as circles of 8-mm diameter (Fig. 1d).

2.2. Animals

The experiments included two types of mice: specific pathogen-free (SPF) male C57BL/6J and BKS.Cg- + Lepr/+Lepr db mice (8–9 weeks old; CLEA Japan Inc., Tokyo, Japan). The mice were housed individually in a temperature-controlled animal facility. The serum glucose cutoff level for inclusion in BKS.Cg- + Lepr/+Lepr db/Jcl mice was 300 mg/dL as per the levels for diabetic mice reported by CLEA Japan Inc. The animal experimental protocol was approved by the Animal Research Committee of Kyoto University Graduate School of Medicine (permit number: Med Kyo 20123). The number of animals used in this study was kept to a minimum, and all possible efforts were made to reduce the suffering of animals in compliance with the protocols established by the Animal Research Committee.

2.3. Surgical procedures

All animal experiments were performed in an SPF clean room in the animal laboratory. The materials were evaluated using a splinted murine wound model that eliminates wound contraction [13]. The mice were placed in a box filled with high concentrations of isoflurane for pre-anesthesia, and anesthesia was maintained using mask inhalation with 1.5–3% isoflurane during subsequent procedures. First, the back hair was shaved with an electric razor and depilated using a depilating cream (Kracie, Tokyo, Japan). Second, a donut-shaped silicone skin splint (Fuji System Corp., Tokyo, Japan) with an outer diameter of 18 mm, inner diameter of 12 mm, and thickness of 0.5 mm was attached to the back using a binding adhesive (Aronalpha®; Daiichi Sankyou Co., Osaka, Japan) and stitched using 5-0 black nylon (Bear Corp., Osaka, Japan). A full-thickness skin defect of 8-mm diameter was prepared at the center of the splint using a punch biopsy tool (Kai Industries Co., Ltd., Tokyo, Japan) and scissors.

We established the following three experimental groups (n = 18 per group): P (Pelnac®), S2.5 (2.5-mm-thick SE sponge), and S5.0 (5.0-mm-thick SE sponge) groups. In the experimental groups, each material was placed on the wound and affixed using a polyurethane film (Tegaderm™; 3 M™, 3 M Japan Ltd., Tokyo, Japan). In the control group (C group, n = 18), the wound was only covered with the polyurethane film. In all groups, the polyurethane film was covered with a sterile gauze and an elastic bandage to protect against contamination and self-mutilation. After these procedures, the mice were placed into individual cages. They were checked every few days and re-fixed under inhalation anesthesia if the bandages had slipped. Each group was further divided into three subgroups (n = 6 per group), and each subgroup was euthanized using carbon dioxide inhalation on postoperative days 7, 14, and 21. Subsequently, the dressing was removed and gross photographs of

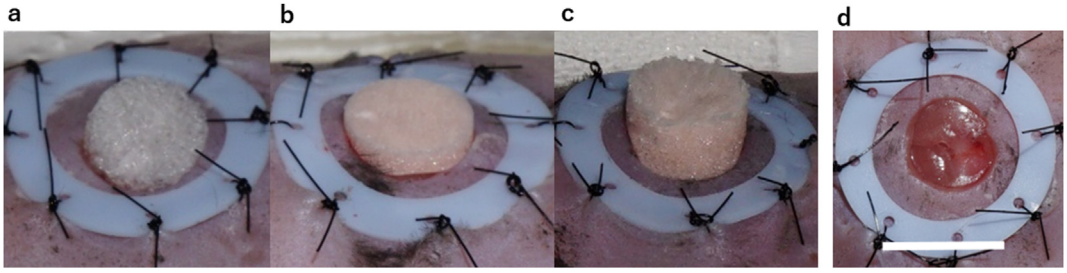

Fig. 1. Materials. (a) Pelnac ® single-layer type, (b) 2.5-mm-thick silk elastin, and (c) 5.0-mm-thick silk elastin tape was applied on the prepared mouse wounds. (d) The wound is 8 mm in diameter. Scale bar = 10 mm.

the wounds were taken using a digital camera (RIKOH Co., Ltd., Tokyo, Japan). The wound was harvested, including the surrounding tissue, divided in half, and one half was fixed in 10% formalin buffer (Wako Pure Chemical Industries, Ltd., Osaka, Japan) for histological staining. The tissues were stored in a polyethylene mesh bag (AS ONE Corp., Osaka, Japan) to preserve their shape. The other half was flash frozen in liquid nitrogen using CryoTube™ (Thermo Fischer Scientific, Waltham, MA, USA) for RNA extraction and real-time polymerase chain reaction (PCR) and stored at −80 °C.

2.4. Histological staining

For immunostaining, tissue sections were deparaffinized and rehydrated, and heat-induced antigen retrieval was performed in ethylenediamine tetraacetic acid (EDTA) (Nichirei Biosciences Inc., Tokyo, Japan) at 98 °C for 20 min. The sections were rinsed in distilled water and immersed in 3% hydrogen peroxide for 10 min at room temperature. Subsequently, the sections were rinsed in distilled water and 50 mM Tris-HCl buffer (TBST; pH, 7.6; 0.05% tween-20, and 0.15 M NaCl). The sections were immersed in 3% bovine serum albumin (BSA) in phosphate-buffered saline (PBS) for 60 min at room temperature. Primary antibodies were applied to the sections and incubated overnight at 4 °C. The sections were then rinsed with TBST. A polymer reagent (Simple Stain Mouse MAX PO; Nichirei Co., Tokyo, Japan) was applied at room temperature for 30 min. The sections were rinsed again in TBST, exposed to 3, 3-diaminobenzidine (DAB; Nichirei Co., Tokyo, Japan) and counterstained with hematoxylin and eosin (HE). A rabbit anti-CD31 monoclonal antibody (ab182981, Abcam; Cambridge, UK; 1:10000 dilution), rabbit anti-CD68 polyclonal antibody (ab125212, Abcam; 1:5000 dilution), and rabbit anti-CD163 polyclonal antibody (ab182422, Abcam; 1:4000 dilution). The concentrations of the primary antibody reagents used for immunostaining were determined by examining the concentrations in a pilot study.

2.5. Evaluation of wound healing

2.5.1. Remaining wound area

The remaining wound area was measured on gross photographs using ImageJ 1.50i (National Institutes of Health, Bethesda, MD, USA). The edges of the wounds were traced to measure the wound area. The size of the wound area on days 7, 14, and 21 was compared with the baseline size, and the results were calculated as a percentage (%) of the original wound size.

2.5.2. Histological evaluation

Neoepithelialization, wound contracture, granulation tissue formation, new capillary formation, increase in macrophages, and the remaining amount of SE were evaluated histologically using an optical microscope (KEYENCE BZ-810 and BZ-II Analyzer, KEYENCE Japan, Osaka, Japan).

Preliminary experiments in C57BL/6J mice revealed complete epithelialization of the wounds by day 21; therefore, wound contracture was evaluated on HE-stained sections on day 21 in C57BL/6J mice. Wound contracture was defined as the linear distance between hair follicles on opposite sides closest to the wound [14,15].

Neoepithelialization was evaluated on HE-stained sections on days 7, 14, and 21 based on the length between the wound edge and the end of the epithelium. The hair follicle nearest to the wound was defined as the wound edge [4]. The length of neoepithelialization was measured by tracing the hair follicle to the tip of the neoepithelialization.

Granulation tissue formation was evaluated using azan-stained sections on days 7, 14, and 21. Newly formed granulation tissue was identified by the nearest hair follicles on opposite sides of the wound edge, the wound floor, and a dense area of purple or fine granules [4]. Obvious material remaining above or within the wound was not considered newly formed granulation. The area of granulation tissue formation was also measured.

Newly formed capillaries were evaluated by counting erythrocytes stained with anti-CD31 antibody [4]. The number and area of stained capillaries in the granulation tissue were counted using macro cell count in a BZ-II Analyzer. An increase in macrophages was evaluated by counting the macrophages stained with anti-CD68 or anti-CD163 antibodies. The former is used as a marker of the total number of macrophages and the latter is used as a marker of M2 macrophages, which have anti-inflammatory properties and promote wound healing. The number of macrophages in granulation tissue was counted using macro cell count.

Immunostaining with an anti-SE antibody was used to analyze the amount of remaining SE. The antibodies were purchased from Sanyo Chemical Industries, Ltd. No product numbers were provided. The area of the DAB-colored SE was then measured.

2.6. RNA isolation and real-time PCR analysis

2.6.1. RNA isolation

(1) The tissue was stored at −80 °C in a 1.5-mL micro tube. Subsequently, 500 μL of TRIzol™ Reagent (Product No. 15596018, Invitrogen™, Carlsbad, CA, USA) was added and homogenized with a biomasher (Nippi Inc., Tokyo, Japan). (2) After the tissue was sufficiently loosened, 500 μL of Trizol was added and incubated at room temperature for 5 min (3) Next, 200 μL of chloroform (NAKALAITESQUE, INC., Kyoto, Japan) was added to the tube, shaken vigorously, and incubated at room temperature for 3 min (4) Subsequently, the tissue was centrifuged at 4 °C and 12,000×*g* for 15 min (5) Only the supernatant containing RNA was transferred to a new micro tube; 200 μL of RNAse-free water and 200 μL of chloroform were added and shaken vigorously for milking. (6) The sample was incubated at room temperature for 3 min and centrifuged at 12,000×*g* for 15 min at 4 °C. (7) Only the supernatant was transferred to a new micro tube; 500 μL of isopropanol (NAKALAITESQUE, INC., Kyoto, Japan) was added and vortexed. (8) The sample was incubated at room temperature for 10 min and centrifuged at 12,000×*g* for 15 min at 4 °C. (9) The supernatant was discarded and the nucleic acid pellet was rinsed with 1 mL ethanol (NAKALAITESQUE, INC.) and centrifuged at 7500×*g* for 5 min at 4 °C (10). The ethanol and air were discarded to dry the pellets. All steps were performed on ice, whenever possible, to prevent RNA damage.

2.6.2. Reverse transcription of cDNA

The extracted RNA was diluted with RNAse-free water SuperScript™ VILO™ cDNA Synthesis Kit (Product No.11754050, Invitrogen™) and reverse-transcribed in a thermal cycler, LifeECO (NIPPON Genetics Co., Ltd., Tokyo, Japan).

2.6.3. Real-time PCR

The synthesized cDNA was diluted to 10 ng/μL with RNAse-free water and used as a template. In a MicroAmp™ Optical 96-Well Reaction Plate (Applied Biosystems™, Foster, CA, USA), 2 μL of the template was mixed with 7 μL of RNAse-free water, 10 μL of TaqPath™ qPCR Master Mix (Applied Biosystems™), and 1 μL of Taqman Gene expression assay (Applied Biosystems™). Automated gene expression analysis was performed using the 7300 Real-Time PCR System (Applied Biosystems™). The TaqMan Gene expression assays used were those for inducible nitric oxide synthase (INOS) (Assay ID: Mm00440502_m1), arginase-1 (ARG1) (Assay ID: Mm00475988_m1), and glyceraldehyde-3-phosphate dehydrogenase (GAPDH) (Assay ID: Mm99999915_g1).

2.7. Statistical analysis

All data are expressed as mean ± standard error and were analyzed using the *t*-test or Tukey–Kramer multiple comparisons test. Statistical significance was defined as $P < 0.05$. JMP15.1 (SAS Institute Japan Ltd, Tokyo, Japan) was used for all analyses. The *t*-test was used only to analyze the remaining amount of SE. The ΔΔCT method was used for real-time PCR analysis.

3. Results

3.1. Remaining wound area

3.1.1. C57BL/6J

Representative gross views of wounds on days 7, 14, and 21 in each group are shown in Fig. 2a. There were no significant differences in the remaining wound areas between the four groups (Fig. 2b).

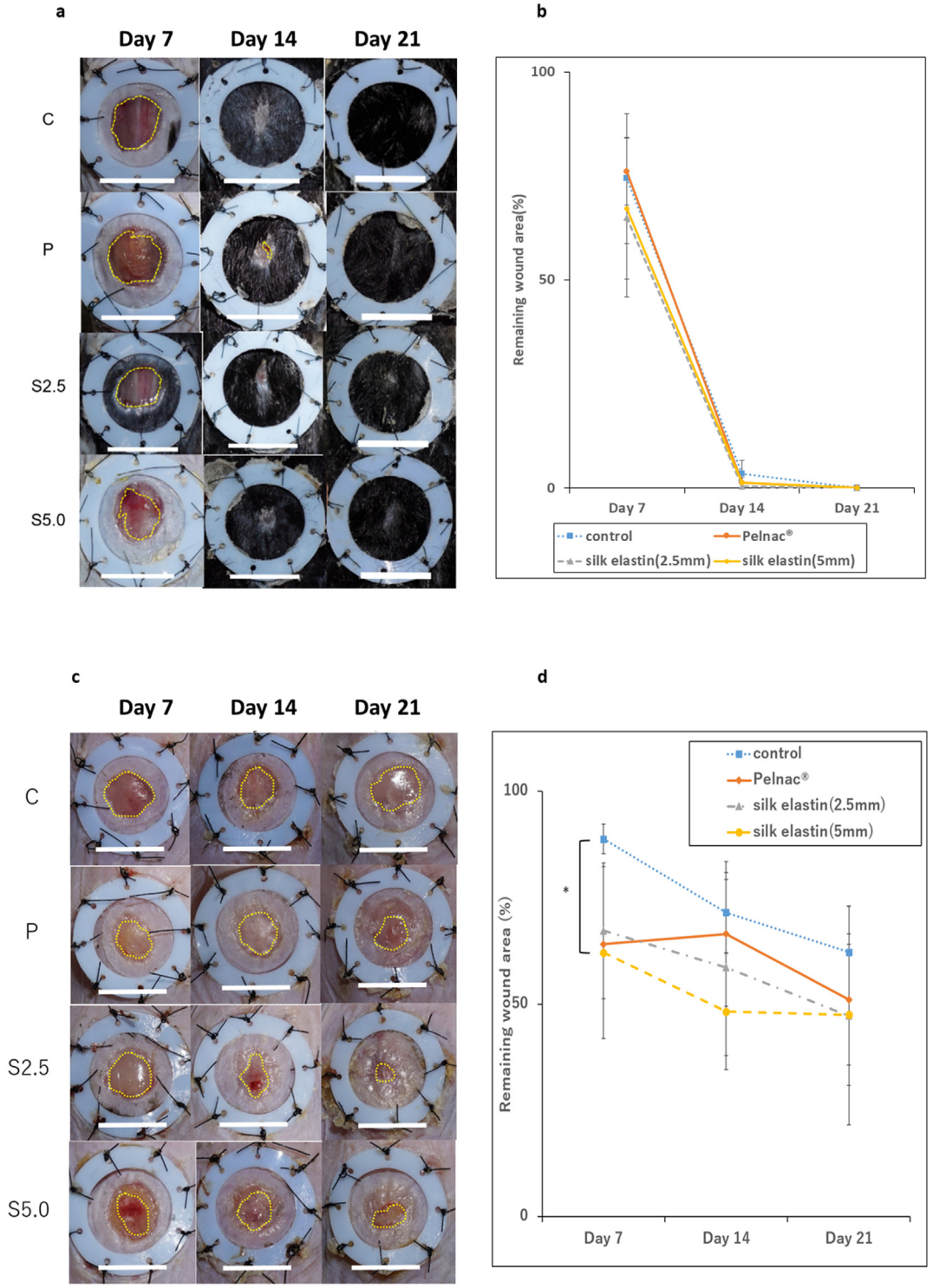

Fig. 2. Remaining wound area. (a) Gross photo of remaining wounds in C57BL/6J mice in each group at days 7, 14, and 21 (yellow broken lines). At day 21, all groups had no residual wounds. Scale bar = 10 mm. (b) There is no significant difference in the remaining wound area between groups. (c) Gross photo of remaining wounds in BKS.Cg- + Lepr/+Lepr db mice in each group on days 7, 14, and 21 (yellow broken lines). Scale bar = 10 mm. (d) On day 7, the S5.0 group had significantly less residual wound area than the C group.

3.1.2. BKS.Cg- + Lepr/+Lepr db

Representative gross views of wounds on days 7, 14, and 21 in each group are shown in Fig. 2c. On day 7, the S5.0 group had a significantly smaller residual wound area than that of the C group (Fig. 2d).

3.2. Wound contracture

HE-stained sections on day 21 in each group are shown in Fig. 3a. There were no significant differences in wound contracture between the four groups (Fig. 3b). However, mice in the C group had more contractures than those in other groups.

3.3. Neoepithelialization

3.3.1. C57BL/6J

HE-stained sections from each group on days 7 and 14 are shown in Fig. 4a. The length of neoepithelialization in S5.0 group was significantly longer than that in the C group on day 7. Additionally, the length of neoepithelialization in the S2.5 and S5.0 groups was significantly longer than that in the control group on day 14 (Fig. 4b). Furthermore, the length of neoepithelialization in the S2.5 and S5.0 groups was longer than that in the P group.

3.3.2. BKS.Cg- + Lepr/+Lepr db

HE-stained sections from each group on days 7, 14, and 21 are shown in Fig. 4c. However, length of neoepithelialization in the S5.0 group was significantly longer than that in the C group on day 7 and those of the other three groups on day 14 (Fig. 4d).

3.4. Granulation tissue formation

3.4.1. C57BL/6J

Azan-stained sections from each group on days 7, 14, and 21 are shown in Fig. 5a. The area of granulation tissue in group S5.0 group was significantly larger than that in the C group on day 7. Granulation tissue area in P group was significantly larger than that in the C group on day 14. The granulation tissue areas in the S5.0 and P groups were significantly larger than those in the C group on day 21 (Fig. 5b).

3.4.2. BKS. Cg- + Lepr/+ Lepr db

Azan-stained sections from each group on days 7, 14, and 21 are shown in Fig. 5c. The area of granulation tissue in the P and S5.0 groups was significantly larger than that in the C group on day 7 (Fig. 5d).

3.5. Newly formed capillaries

3.5.1. C57BL/6J

Micrographs of anti-CD31-stained sections on days 7, 14, and 21 in each group are shown in Fig. 6a. On day 14, the number of newly formed capillaries was significantly higher in the S2.5 group than that in the C group. On day 21, the number and area of newly formed capillaries were significantly higher in the P and S5.0 groups compared to those in the C group (Fig. 6b and c).

3.6. BKS. Cg- + Lepr/+Lepr db

Micrographs of anti-CD31-stained sections on days 7, 14, and 21 in each group are shown in Fig. 6d. On day 14, the number and area of newly formed capillaries were significantly higher in the S5.0 group compared to those in the other three groups (Fig. 6e and f).

3.7. Increase in anti-CD68 antibody-positive macrophages

3.7.1. C57BL/6J

Micrographs of anti-CD68-stained sections on days 7, 14, and 21 in each group are shown in Fig. 7a. On day 7, the S5.0 group had significantly more macrophages than the other groups. On days 14 and 21, the S5.0 and P groups had significantly more macrophages than the C group (Fig. 7b).

3.7.2. BKS.Cg- + Lepr/+Lepr db

Micrographs of anti-CD68-stained sections on days 7, 14, and 21 in each group are shown in Fig. 7c. On day 14, the S5.0 group had a significant increase in total macrophages compared with the P and C groups. On day 21, the P group had a significant increase in total macrophages compared with the S2.5 group (Fig. 7d).

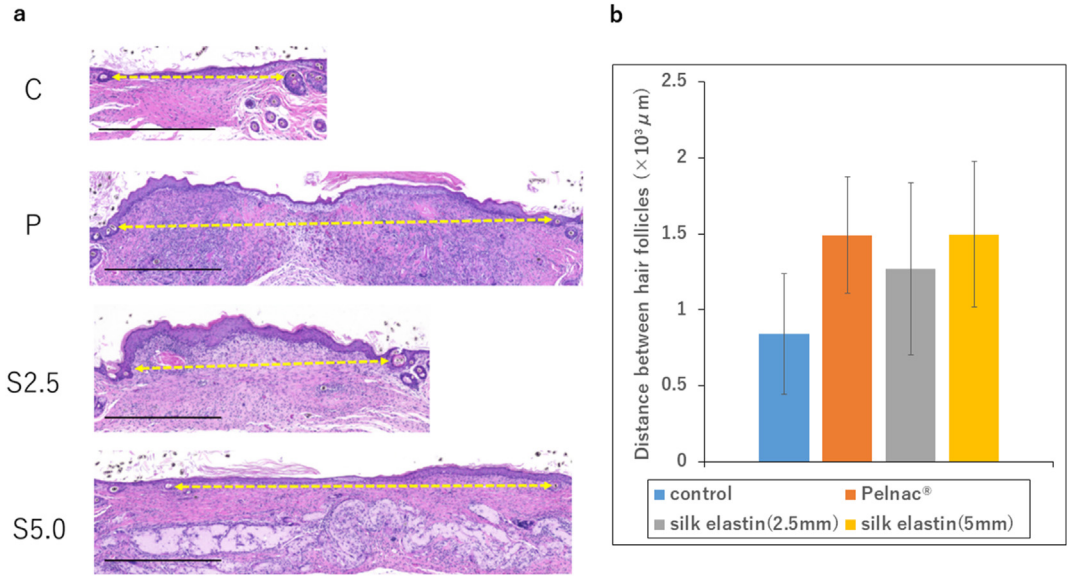

Fig. 3. Wound contracture. (a) Hematoxylin and eosin-stained sections on day 21. The interfollicular linear distance is depicted by the yellow arrow dotted line. Scale bar = 500 μm. (b) There is no significant difference in wound contracture between the groups.

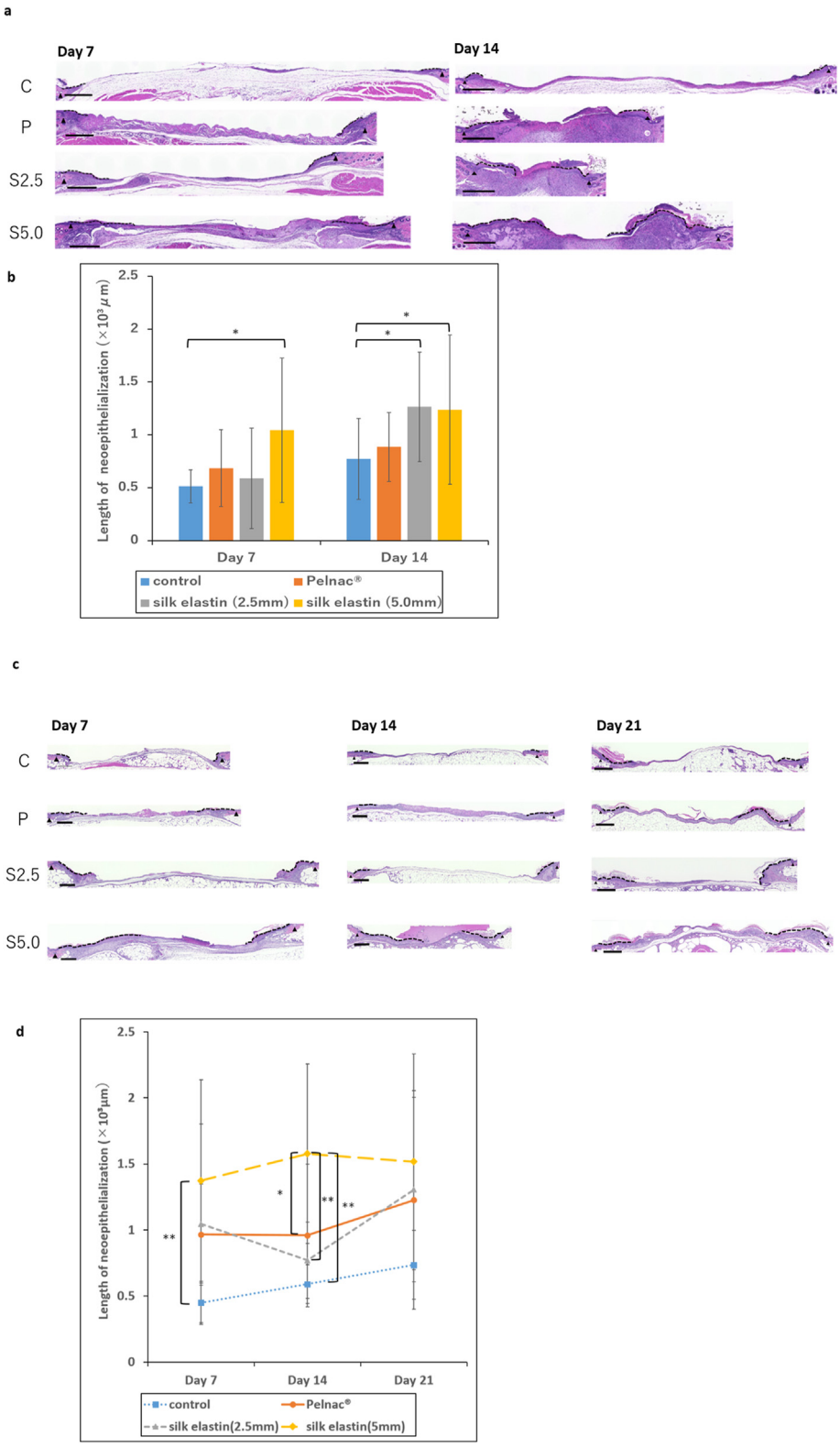

Fig. 4. Neoepithelialization. (a) Hematoxylin and eosin (HE)-stained sections in C57BL/6J mice on days 7 and 14. The length of neoepithelialization is indicated by the dotted black line. The follicle, defined as the wound edge, is indicated by a black triangle. Scale bar = 500 μm. (b) The length of neoepithelialization is significantly greater in the S5.0 group than that in the C group on day 7 and in the S2.5 and S5.0 groups than that in the C group on day 14 (*P < 0.05) (c) HE-stained sections in BKS.Cg- + Lepr/+Lepr db mice on days 7, 14, and 21. The length of neoepithelialization is indicated by the dotted black line. The follicle, defined as the wound edge, is indicated by a black triangle. Scale bar = 500 μm. (d) The length of neoepithelialization is significantly greater in the S5.0 group than that in the C group on day 7 and in the S5.0 group than that in the other three groups on day 14 (*P < 0.05, **P < 0.01).

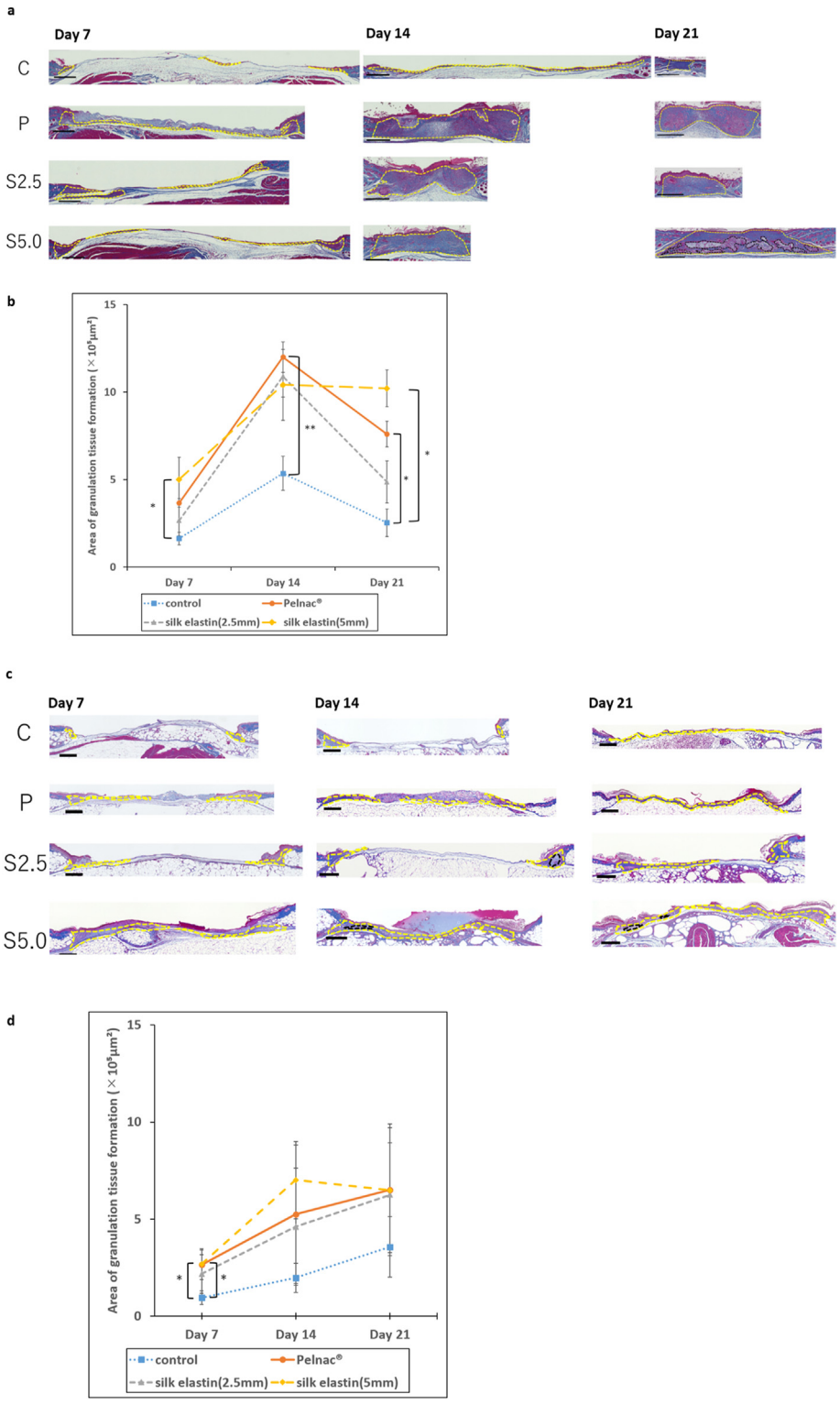

Fig. 5. Granulation tissue formation. (a) Azan-stained sections in C57BL/6J mice on days 7, 14, and 21. The granulation tissue formation area is indicated by the yellow dotted line. Remaining silk elastin is seen in the area circled by the black dotted line. It was not identified as granulation tissue. Scale bar = 500 μm. (b) The granulation area was significantly larger in the S5.0 group than that in the C group on day 7, in the P group than that in the C group on day 14, and in the S5.0 and P groups than that in the C group on day 21 (*P < 0.05). (c) Azan-stained sections in BKS.Cg- + Lepr/+Lepr db mice on days 7, 14, and 21. The granulation tissue formation area is indicated by the yellow dotted line. Remaining silk elastin is seen in the area circled by the black dotted line. It was not identified as granulation tissue. Scale bar = 500 μm. (d) The granulation area was significantly larger in the P and S5.0 groups than that in the C group on day 7 (*P < 0.05).

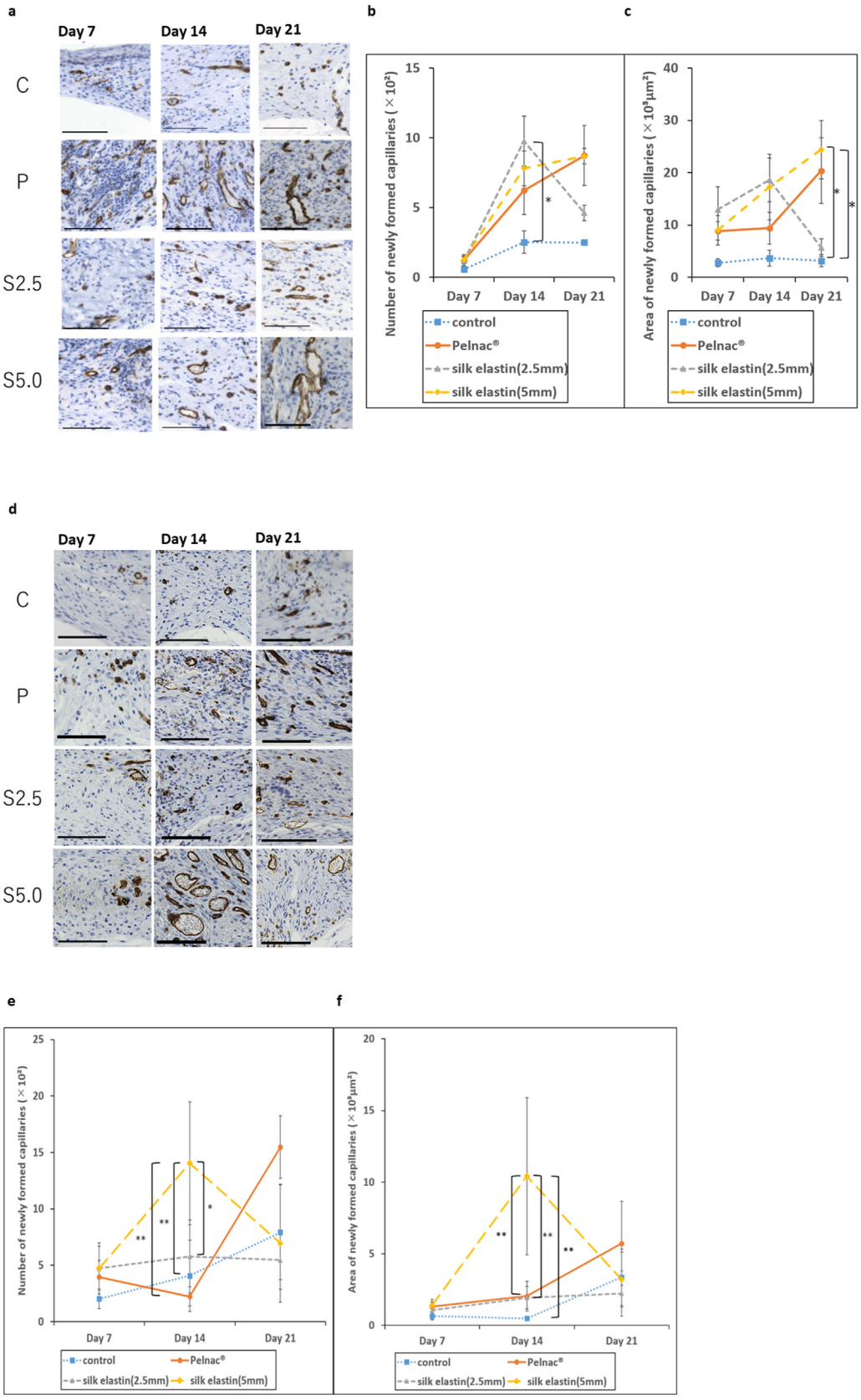

Fig. 6. Newly formed capillaries. (a) Sections immunostained with anti-CD31 antibodies in C57BL/6J mice on days 7, 14, and 21. Scale bar = 100 μm. (b) The number of newly formed capillaries is significantly increased in the S2.5 group compared to that in the C group on day 14 (*P < 0.05). (c) The area of newly formed capillaries is significantly increased in the S5.0 and P groups compared to that in the C group on day 21 (*P < 0.05). (d) Sections immunostained with anti-CD31 antibodies in BKS.Cg- + Lepr/+Lepr db mice on days 7, 14, and 21. Scale bar = 100 μm. (e) The number of newly formed capillaries is significantly increased in the S5.0 group compared to that in the other three groups on day 14 (*P < 0.05, **P < 0.01). (f) The area of newly formed capillaries is significantly increased in the S5.0 group compared to that in the other three groups on day 14 (*P < 0.05, **P < 0.01).

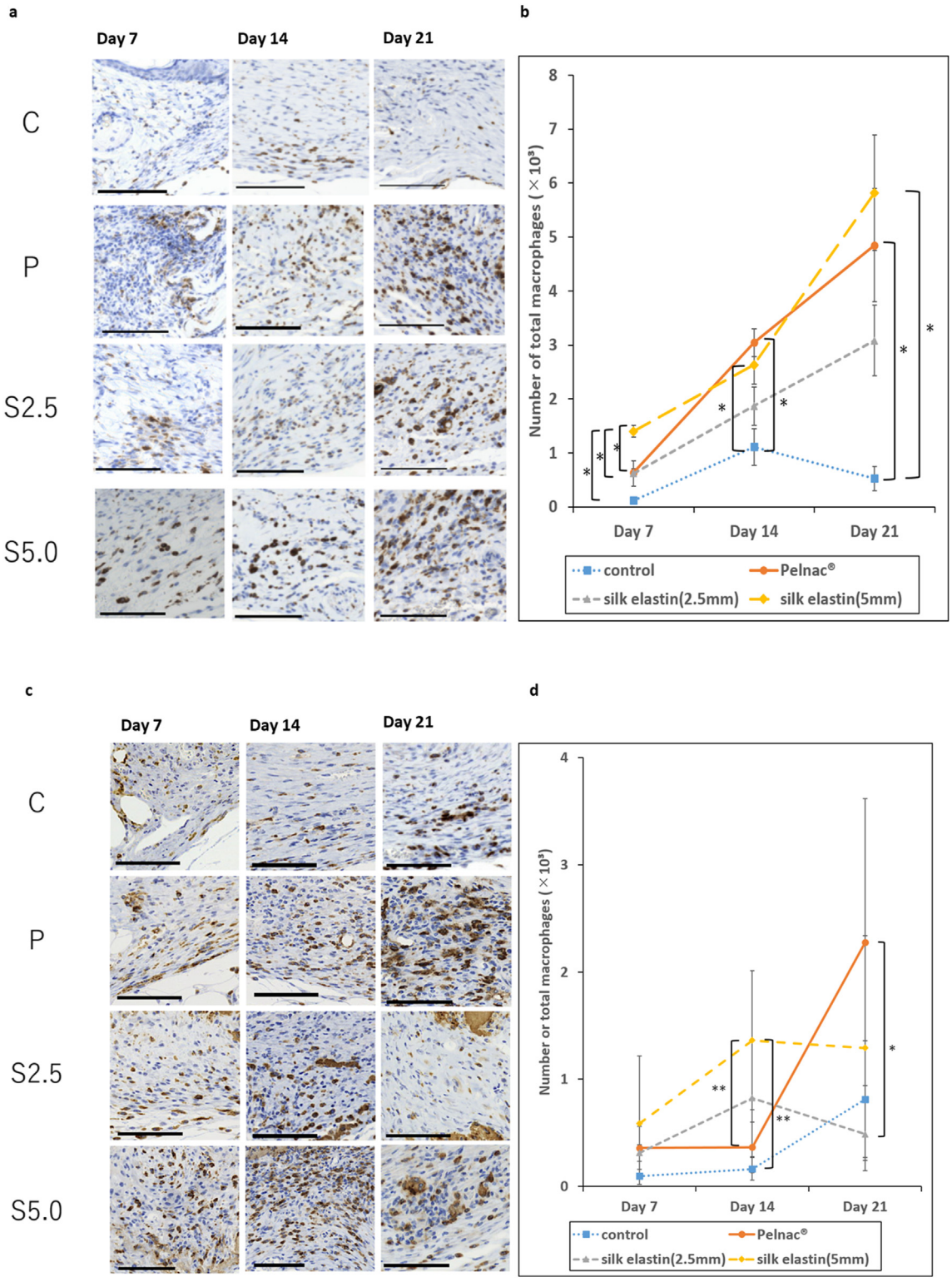

Fig. 7. Increase in the total number of macrophages. (a) Sections immunostained with anti-CD68 antibodies in C57BL/6J mice on days 7, 14, and 21. Scale bar = 100 μm. (b) The number of macrophages is significantly increased in the S5.0 group compared to that in the other groups on day 7, and in the S5 and P groups compared to that in the C group on days 14 and 21 (*P < 0.05). (c) Sections immunostained with anti-CD68 antibodies in BKS.Cg- + Lepr/+Lepr db mice on days 7, 14, and 21. Scale bar = 100 μm. (d) The number of macrophages is significantly increased in the S5.0 group compared to those in the P and C groups on day 14, and in the P group compared to that in the S2.5 group on day 21 (*P < 0.05, **P < 0.01).

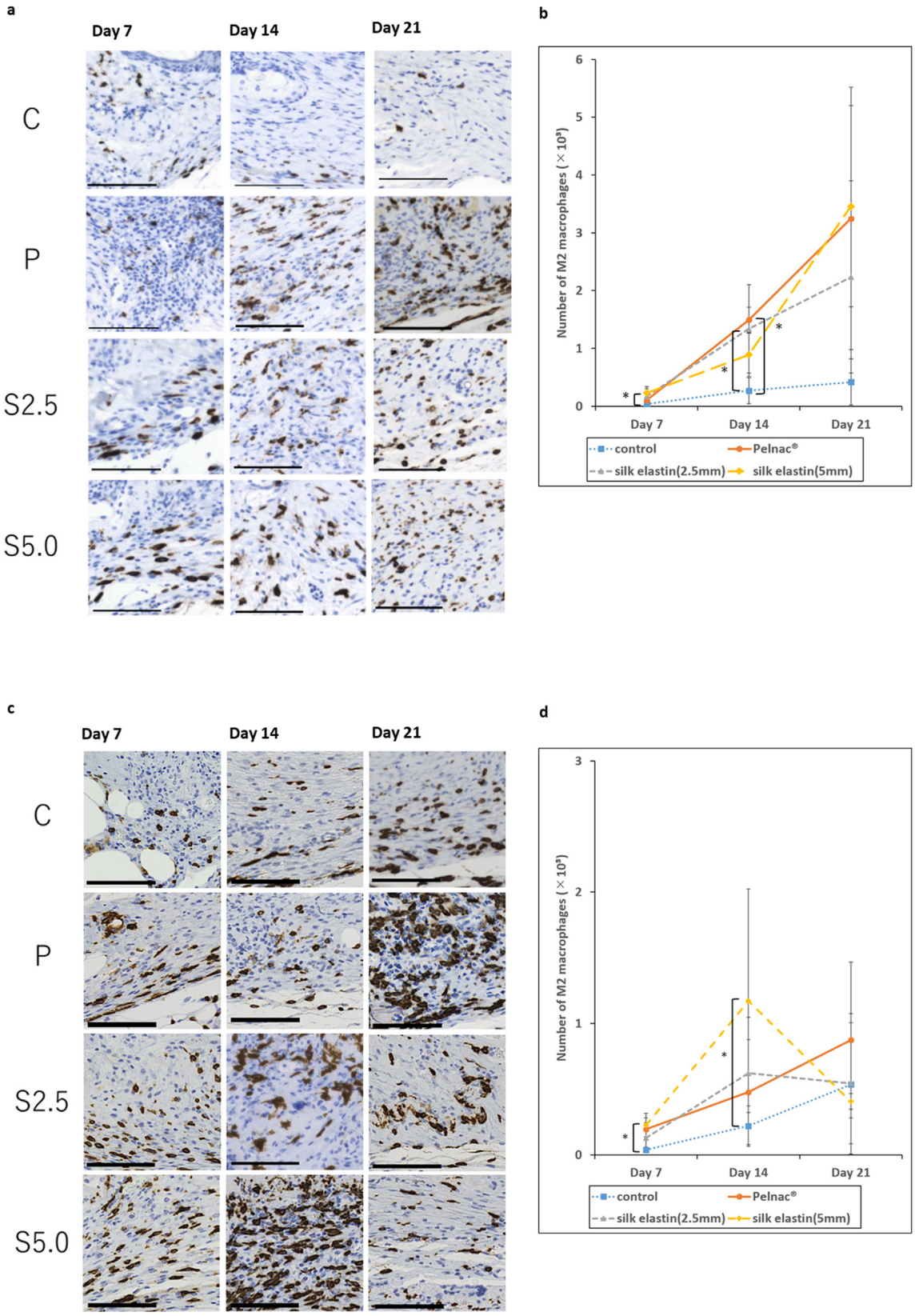

Fig. 8. Increase in the number of M2 macrophages. (a) Sections immunostained with anti-CD163 antibodies in C57BL/6J mice on days 7, 14, and 21. Scale bar = 100 μm. (b) The number of M2 macrophages is significantly increased in the S5.0 group compared with that in the C group on day 7, and in the S2.5 and P groups compared with that in the C group on day 14 (*P < 0.05). (c) Sections immunostained with anti-CD163 antibodies in BKS.Cg- + Lepr/+Lepr db mice at days 7, 14, and 21. Scale bar = 100 μm. (d) The number of M2 macrophages is significantly increased in the S5.0 group compared to that in the C group on days 7 and 14 (*P < 0.05).

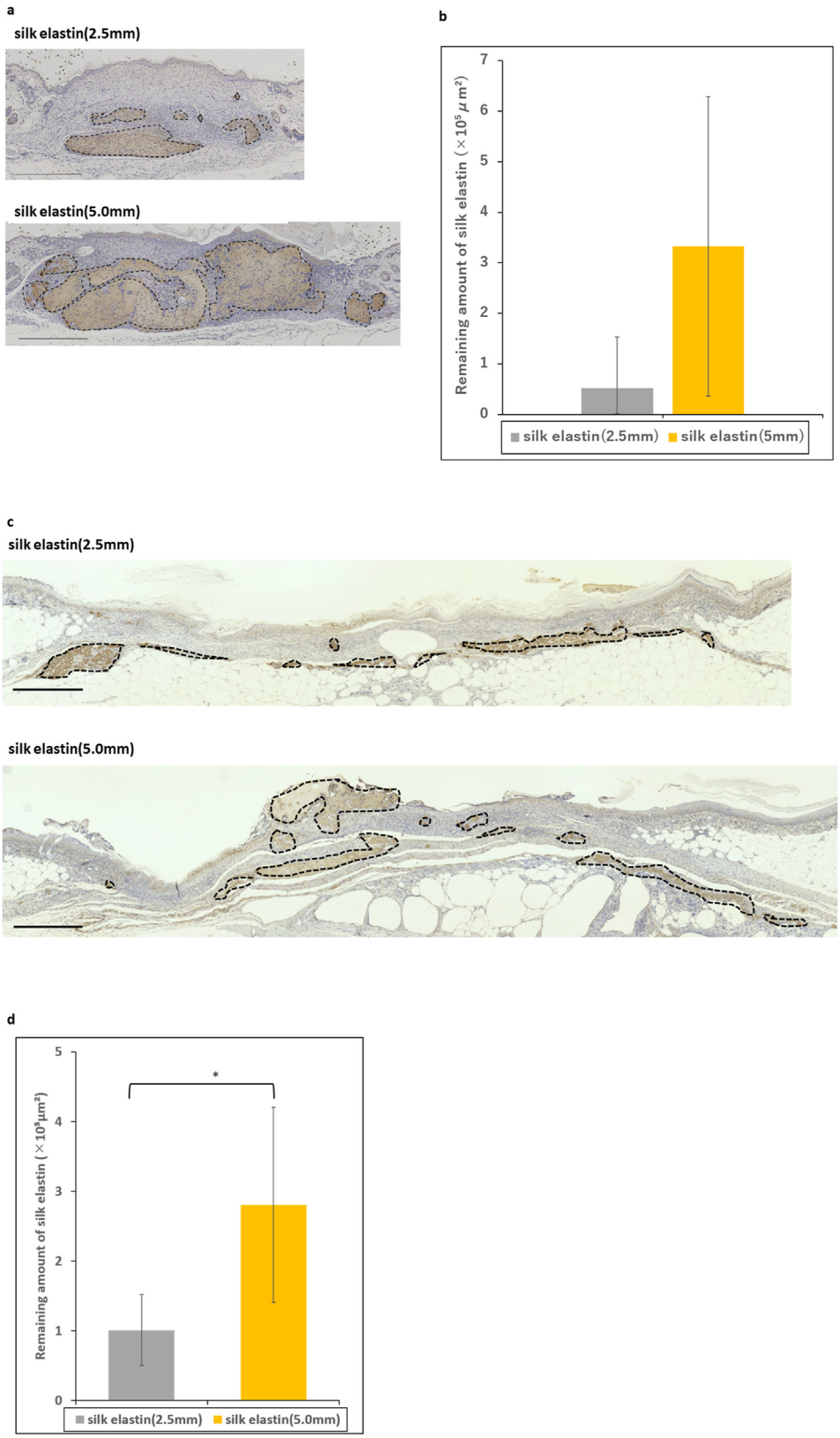

Fig. 9. Remaining amount of silk elastin on day 21. (a) Remaining silk elastin in the wounds of C57BL/6J mice is indicated by the black dotted line. Scale bar = 500 μm. (b) The remaining amount varied, and no significant difference was found. (c) Remaining silk elastin in wounds of BKS.Cg- + Lepr/+Lepr db mice is indicated by the black dotted line. Scale bar = 500 μm. (d) The amount of remaining silk elastin was significantly higher in the S5.0 group on day 21. In the S5.0 group (*P < 0.05), however, the remaining amount of silk elastin varied.

3.8. Increase in anti-CD163 antibody-positive macrophages

3.8.1. C57BL/6J

Micrographs of anti-CD163-stained sections on days 7, 14, and 21 in each group are shown in Fig. 8a. On day 7, the S5.0 group had significantly more macrophages than the C group. On day 14, the S2.5 and P groups had significantly more macrophages than the C group (Fig. 8b).

3.8.2. BKS. Cg- + Lepr/+Lepr db

Micrographs of anti-CD163-stained sections on days 7, 14, and 21 in each group are shown in Fig. 8c. On days 7 and 14, the S5.0 group had significantly more macrophages than the C group (Fig. 8d).

3.9. Remaining amount of SE

3.9.1. C57BL/6J

The amount of SE remaining on day 21 is shown in Fig. 9a. There was a large variation in the amount of remnant SE; however, no significant difference was observed between the two SE thickness groups (Fig. 9b).

3.9.2. BKS.Cg- + Lepr/+Lepr db

The amount of SE remaining on day 21 is shown in Fig. 9c. There was a large variation in the remaining amount of SE; there was a significantly larger amount in theS5.0 group than that in the S2.5 group (Fig. 9d).

3.10. Real-time PCR

INOS gene expression was significantly higher in the S5.0 group than that in the C group on day 7 and in the S5.0 group than that in the S2.5 group on day 14 (Fig. 10a). ARG1 expression was significantly higher in the S5.0 group than that in the C group on day 14 (Fig. 10b).

4. Discussion

In this study, we investigated the efficacy of SE sponges in wound healing and compared it with that of collagen sponges. Although differences between the groups were unclear in C57BL/6J mice, they were evident in BKS.Cg- + Lepr/+Lepr db mice. Our findings suggest that on wounds, SE sponges behave differently than collagen sponges. While collagen sponges act as a scaffold in wounds and are gradually replaced by granulation tissue, SE sponges get fragmented and their gel residues undergo changes, as observed with azan and SE antibody staining. Despite these differences, SE sponges were comparable to collagen sponges in promoting wound healing. Additionally, the significant differences in epithelialization and angiogenesis observed with different thicknesses of the SE sponges may indicate its volume-based efficacy.

Macrophages play a crucial role in the wound healing process [16–18]. When tissue injury occurs, inflammatory macrophages (commonly referred to as “M1” macrophages) initially infiltrate the wound site and work toward eliminating bacteria, foreign substances, and dead cells. As the tissue healing process begins, the entire macrophage population shifts to a state that promotes anti-inflammatory activity (collectively referred to as “M2” macrophages). Subsequently, fibroblasts, keratinocytes, and endothelial cells migrate and proliferate, respectively, to promote dermis, epidermis, and vasculature repair.

In vitro studies have indicated that silk elastin can enhance macrophage migration [19] and induce differentiation into M2 macrophages [20]. Based on these findings, we hypothesized that increased macrophage migration triggered by silk elastin potentially enhances wound healing. To explore this, we evaluated behavior of macrophages within the wound using histological and real-time PCR analyses. For histological assessment, CD68-positive cells were categorized as all macrophages and CD163-positive cells as M2 macrophages. CD68 staining showed that silk elastin significantly increased macrophages in the wound, consistent with the study by Ozaki et al. [19]. Similarly, CD163 staining indicated a tendency toward increase in M2 macrophages consistent with the study by Unzai et al. [20]. In the real-time PCR analysis, INOS served as a marker for M1 macrophages, while ARG1 was used for M2 macrophages. Both markers exhibited a tendency for increased gene expression in response to silk elastin. The increased macrophage migration may explain the extended initial neo epithelialization observed in wounds treated with SE sponges since adequate macrophage migration is crucial for enhanced epithelialization. This finding is supported by existing small animal studies demonstrating that the rapid progression of a wound healing cascade promotes epithelialization [21]. Additionally, Li et al. reported that macrophage-derived exosomes promoted epithelialization in a diabetic rat model through anti-inflammatory effects [22].

SE sponges can form a gel on wounds, thus allowing them to adapt to complex wound surfaces like hydrogels, such as Granugel® and Intracite Gel®. However, the wound-healing mechanism of SE sponges appears to be different from that of hydrogels and should be used according to the wound characteristics. Hydrogels

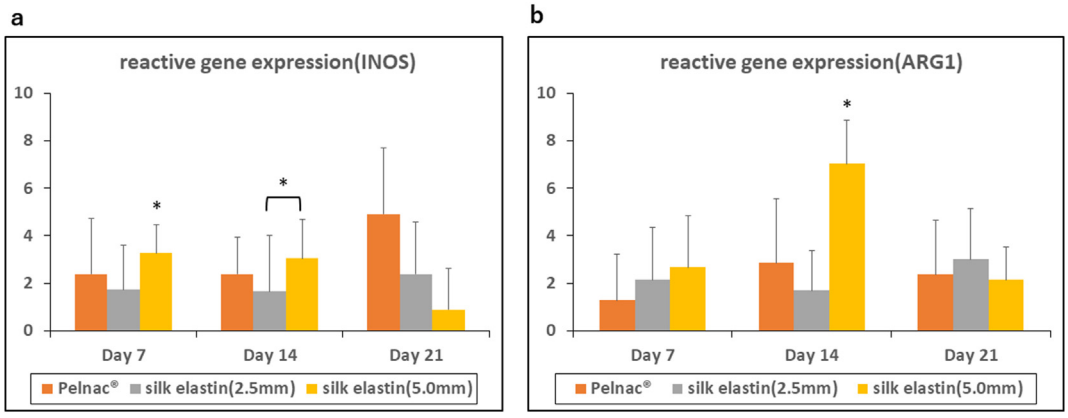

Fig. 10. Real-time polymerase chain reaction (PCR). (a) The expression level of INOS was analyzed using the C group as the control. The expression level in the S5.0 group was significantly higher than that in the C group on day 7, and the expression level in the S5.0 group was significantly higher than that in the S2.5 group on day 14 (*P < 0.05). (b) ARG1 expression was analyzed with comparison to that in the C group. On day 14, the expression in the S5.0 group was significantly higher than that in the C group (*P < 0.05).

can promote the autodigestion of necrotic tissue by maintaining tissue hydration; however, SE sponges may not be suitable for wounds with necrotic tissue because any excess exudate inhibits SE gelation [23,24]. As noted in a clinical study by Noda et al. [12], SE should be applied after the exudate has subsided to achieve optimal wound healing outcomes. Nevertheless, SE sponges may have other applications because of their superiority in inhibiting bacterial growth as reported by Kawai et al. [9].

A limitation of this study is the lack of animal blinding and sample size calculations. Real-time PCR was also performed in C57BL/6J mice; however, the results did not support the main argument, and further genetic analyses are warranted. Additionally, value variations between individual mice were large, and further studies using larger animal models with sufficient sample sizes are needed to evaluate the reproducibility and validity of our results.

5. Conclusion

The wound-healing effects of SE sponge were compared with those of collagen sponge in murine wound models. SE did not function as a scaffold but promoted early macrophage migration and tended to have better initial neoepithelialization and angiogenesis. Although further studies are required, SE sponges have the potential to be used as a novel dressing for wounds.

Funding

This study was supported by the National Institute of Biomedical Research and Development (Control No.: 01-303).

Declaration of competing interest

The authors declare that they have no conflict of interest.

Acknowledgements

The silk elastin sponge was provided by Kawabata. Anti-silk elastin staining was performed by Sanyo Chemical Industries Ltd.

References

[1] Winter GD. Formation of the scab and the rate of epithelization of superficial wounds in the skin of the young domestic pig. Nature 1962;193:293–4.
[2] Nuutila K, Eriksson E. Moist wound healing with commonly available dressings. Adv Wound Care 2021;10(12):685–98.
[3] Morimoto N, Yoshimura K, Niimi M, Ito T, Aya R, Fujitaka J, et al. Novel collagen/gelatin scaffold with sustained release of basic fibroblast growth factor: clinical trial for chronic skin ulcers. Tissue Eng 2013;19(17–18):1931–40.
[4] Notodihardjo SC, Morimoto N, Munisso MC, Le TM, Mitsui T, Kakudo N, et al. A comparison of the wound healing process after the application of three dermal substitutes with or without basic fibroblast growth factor impregnation in diabetic mice. J Plast Reconstr Aesthetic Surg 2020;73(8):1547–55.
[5] Cappello J, Crissman J, Dorman M, Mikolajczak M, Textor G, Marquet M, et al. Genetic engineering of structural protein polymers. Biotechnol Prog 1990;6(3):198–202.
[6] Litwiniuk M, Grzela T. Amniotic membrane: new concepts for an old dressing. Wound Repair Regen 2014;22(4):451–6.
[7] Urry DW. Entropic elastic processes in protein mechanisms. I. Elastic structure due to an inverse temperature transition and elasticity due to internal chain dynamics. J Protein Chem 1988;7(1):1–34.
[8] Cappello J, Crissman JW, Crissman M, Ferrari FA, Textor G, Wallis O, et al. In-situ self-assembling protein polymer gel systems for administration, delivery, and release of drugs. J Contr Release 1998;53(1–3):105–17.
[9] Kawai K, Kanda N, Kawabata S, Suzuki S. The effect of silk-elastin in the pressure ulcers. Jpn JPU 2013;15(1):41–7.
[10] Kawabata S, Kawai K, Somamoto S, Noda K, Matsuura Y, Nakamura Y, et al. The development of a novel wound healing material, silk-elastin sponge. J Biomater Sci Polym Ed 2017;28(18):2143–53.
[11] Kawabata S, Kanda N, Hirasawa Y, Noda K, Matsuura Y, Suzuki S, et al. The Utility of silk-elastin hydrogel as a new material for wound healing. Plast Reconstr Surg Glob Open 2018;6(5):e1778.
[12] Noda K, Kawai K, Matsuura Y, Ito-Ihara T, Amino Y, Ushimaru M, et al. Safety of silk-elastin sponges in patients with chronic skin ulcers: a Phase I/II, single-center, open-label, single-arm clinical trial. Plast Reconstr Surg Glob Open 2021;9(4):e3556.
[13] Galiano RD, Michaels J, Dobryansky M, Levine JP, Gurtner GC. Quantitative and reproducible murine model of excisional wound healing. Wound Repair Regen 2004;12(4):485–92.
[14] Morimoto N, Saso Y, Tomihata K, Taira T, Takahashi Y, Ohta M, et al. Viability and function of autologous and allogeneic fibroblasts seeded in dermal substitutes after implantation. J Surg Res 2005;125(1):56–67.
[15] Notodihardjo PV, Morimoto N, Kakudo N, Matsui M, Sakamoto M, Liem PH, et al. Gelatin hydrogel impregnated with platelet-rich plasma releasate promotes angiogenesis and wound healing in murine model. J Artif Organs 2015;18(1):64–71.
[16] Mosser DM, Edwards JP. Exploring the full spectrum of macrophage activation. Nat Rev Immunol 2008;8(12):958–69.
[17] Ferrante CJ, Leibovich SJ. Regulation of macrophage polarization and wound healing. Adv Wound Care 2012;1(1):10–6.
[18] Krzyszczyk P, Schloss R, Palmer A, Berthiaume F. The role of macrophages in acute and chronic wound healing and interventions to promote pro-wound healing phenotypes. Front Physiol 2018;9:419.
[19] Ozaki C, Somamoto S, Kawabata S, Tabata Y. Effect of an artificial silk elastin-like protein on the migration and collagen production of mouse fibroblasts. J Biomater Sci Polym Ed 2014;25(12):1266–77.
[20] Unzai T, Washisaka T, Tabata Y. An artificial silk elastin-like protein modifies the polarization of macrophages. ACS Appl Bio Mater 2022;5(12):5657–64.
[21] El Masry MS, Chaffee S, Ghatak PD, Mathew-Steiner SS, Das A, Higuita-Castro N, et al. Stabilized collagen matrix dressing improves wound macrophage function and epithelialization. Faseb J 2019;33(2):2144–55.
[22] Li M, Wang T, Tian H, Wei G, Zhao L, Shi Y, et al. Macrophage-derived exosomes accelerate wound healing through their anti-inflammation effects in a diabetic rat model. Artif Cells, Nanomed Biotechnol 2019;47(1):3793–803.
[23] Williams C. Intrasite Gel: a hydrogel dressing. Br J Nurs 1994;3(16):843–6.
[24] Williams C. Granugel: hydrocolloid gel. Br J Nurs 1996;5(3):188–90.